Applied and Environmental Microbiology, May 2008, p. 2841–2851 Vol. 74, No. 9
0099-2240/08/$08.00+0 doi:10.1128/AEM.02027-07

Impact of Nitrate on the Structure and Function of Bacterial Biofilm Communities in Pipelines Used for Injection of Seawater into Oil Fields▽†

Carsten U. Schwermer,[1]* Gaute Lavik,[1] Raeid M. M. Abed,[1] Braden Dunsmore,[2]‡ Timothy G. Ferdelman,[1] Paul Stoodley,[3] Armin Gieseke,[1] and Dirk de Beer[1]

Max Planck Institute for Marine Microbiology, Celsiusstrasse 1, D-28359 Bremen, Germany[1]; Oil Plus, Ltd., Kennet Side, Newbury, Berkshire RG14 5PX, United Kingdom[2]; and Center for Genomic Sciences, Allegheny-Singer Research Institute, 320 East North Avenue, Pittsburgh, Pennsylvania 15212-4772[3]

Received 4 September 2007/Accepted 3 March 2008

We studied the impact of NO_3^- on the bacterial community composition, diversity, and function in in situ industrial, anaerobic biofilms by combining microsensor profiling, ^{15}N and ^{35}S labeling, and 16S rRNA gene-based fingerprinting. Biofilms were grown on carbon steel coupons within a system designed to treat seawater for injection into an oil field for pressurized oil recovery. NO_3^- was added to the seawater in an attempt to prevent bacterial H_2S generation and microbially influenced corrosion in the field. Microprofiling of nitrogen compounds and redox potential inside the biofilms showed that the zone of highest metabolic activity was located close to the metal surface, correlating with a high bacterial abundance in this zone. Upon addition, NO_3^- was mainly reduced to NO_2^-. In biofilms grown in the absence of NO_3^-, redox potentials of < -450 mV at the metal surface suggested the release of Fe^{2+}. NO_3^- addition to previously untreated biofilms induced a decline (65%) in bacterial species richness, with *Methylophaga*- and *Colwellia*-related sequences having the highest number of obtained clones in the clone library. In contrast, no changes in community composition and potential NO_3^- reduction occurred upon subsequent withdrawal of NO_3^-. Active sulfate reduction was below detection levels in all biofilms, but S isotope fractionation analysis of sulfide deposits suggested that it must have occurred either at low rates or episodically. Scanning electron microscopy revealed that pitting corrosion occurred on all coupons, independent of the treatment. However, uniform corrosion was clearly mitigated by NO_3^- addition.

Biofilms are matrix-embedded communities of microorganisms attached to an interface (usually solid-liquid). They represent an important mode for bacterial growth in natural, medical, and industrial ecosystems (18, 24, 57). Their appearance can be either beneficial or detrimental. In engineered systems, such as wastewater treatment, cooling water systems, and food processing, biofilms cause problems for the particular operation (20). In the oil industry, deoxygenated seawater is often injected into reservoirs for secondary oil recovery and pressure maintenance. Biofilms adherent to surfaces within these injection systems and in the reservoir harbor diverse communities of bacteria. They cause significant operational problems due to fouling, corrosion of iron and steel alloys, reduction of flow, souring (contamination of oil and gas by bacterially generated sulfide), and reservoir plugging (20, 61). Biofilms may provide niches for sulfate-reducing bacteria (SRB) that form hydrogen sulfide (H_2S) from sulfate-containing seawater. H_2S is toxic, corrodes surfaces in pipelines and other equipment, and reduces the quality of oil and gas, therefore causing great financial losses worldwide.

Biocides are frequently used to control the growth of biofilms in such systems, particularly to inhibit SRB and other corrosive microorganisms. However, the effect of biocides is limited, and due to environmental risks, their use is restricted. A more environmentally sound and potentially cost-efficient approach based on the addition of NO_3^- or NO_2^- to injection waters (i.e., waters used for injection into oil and gas fields) to control souring has been applied in the field with variable results (16, 33, 60, 65, 66). Several mechanisms have been proposed for NO_3^-/NO_2^--mediated souring control: (i) outcompetition of SRB by NO_3^-/NO_2^--reducing bacteria (NRB) for available electron donors; (ii) inhibition of SRB by NO_3^- reduction products (i.e., NO_2^- and NO) from heterotrophic NRB and/or autotrophic NR sulfide-oxidizing bacteria; (iii) switch of some SRB from SO_4^{2-} reduction to dissimilatory NO_3^- reduction to ammonium (DNRA); (iv) removal of H_2S through H_2S oxidation with NO_3^- as electron acceptor by NR sulfide-oxidizing bacteria (15, 19, 27, 41, 44, 50).

NO_3^-/NO_2^- treatment of oil field reservoirs may also prevent or mitigate microbially influenced corrosion (MIC) in the production facilities, including pipelines (64). The impact of this treatment and the long-term consequences for MIC are poorly understood. Field investigations on NO_3^-/NO_2^- efficacy for souring and corrosion control have previously focused on planktonic communities, cell suspensions, or debris instead of substrate-attached intact biofilms (34, 64). However, main-

* Corresponding author. Mailing address: Max Planck Institute for Marine Microbiology, Celsiusstrasse 1, 28359 Bremen, Germany. Phone: 49 4212028 838. Fax: 49 4212028 690. E-mail: cschwerm@mpi-bremen.de.

‡ Present address: Baker Petrolite, Level 7, 256 St. Georges Terrace, Perth, WA 6000, Australia.

† Supplemental material for this article may be found at http://aem.asm.org/.

▽ Published ahead of print on 14 March 2008.

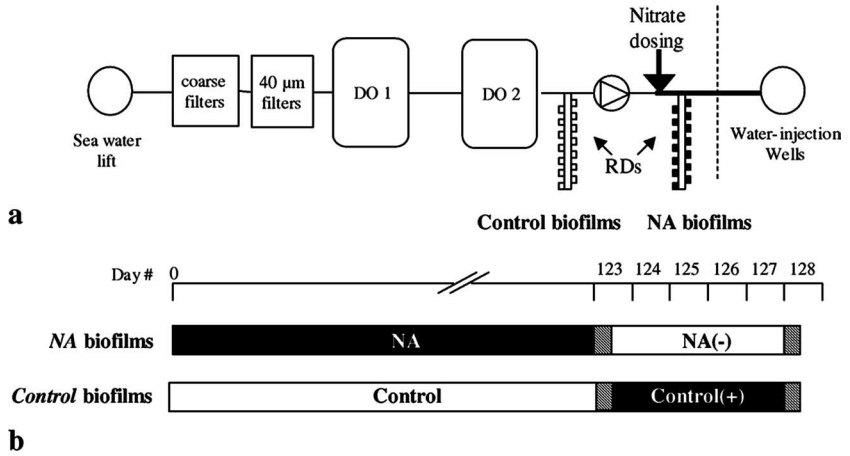

FIG. 1. (a) Positions of RD in the seawater deoxygenation (DO) system. O_2 was removed from the water in a two-stage gas-stripping process after filtration. (b) Schematic diagram of the experimental treatments. Black and white bars indicate exposure to NO_3^--rich (1 mM; NA biofilms) and NO_3^--free (control biofilms) seawater, respectively. RD were exchanged to opposite conditions on day 123. ^{15}N and ^{35}S tracer incubations were done on days 123 and 128 (hatched bars).

taining the structural integrity of biofilms is necessary for understanding mass transfer in the biofilms and cell-cell and cell-environment interactions, as well as the processes and conditions causing corrosion problems owing to MIC. Local concentrations of NO_3^- and its reduction products inside the biofilms are unknown but are essential for evaluating the effectiveness of the treatment, as is the in situ impact of NO_3^- on a complex bacterial community.

We investigated biofilms derived from an injection system that prepared anoxic seawater. NO_3^- was added to the water that was transported via a 9-km-long subsea pipeline to the injection well, where it was pumped into the field. Until injection commenced 4 years prior to the study, no significant amounts of H_2S had been detected in the injection water. However, since SRB had previously been found in biofilm debris obtained from the injection pipeline (34), it was important to ascertain whether those or other bacteria continued to grow even in the presence of NO_3^- and if bacteria or the treatment itself induced corrosion in the injector and pipelines. Microsensor profiling was combined with ^{15}N and ^{35}S labeling, 16S rRNA gene-based fingerprinting, and sulfur isotope fractionation in order to (i) link structure and function in the injection water biofilms; (ii) identify dominant bacteria therein; (iii) assess the impact of short- and long-term NO_3^- exposure on the bacterial community composition, diversity, and function; and (iv) identify potential corrosion damage and deposits underlying the biofilms.

MATERIALS AND METHODS

Biofilm establishment and system conditions. Biofilms were grown inside an offshore water injection system being treated with NO_3^- at an oil field in the North Sea. Removable carbon steel coupons (0.2-cm^2 surface area) made from the same structural pipeline material were mounted in Robbins devices (RD) to facilitate in situ sampling of biofilms grown on the coupons. The steel was marine grade, low-alloy mild steel (AISI 1018) typically containing 0.15 to 0.2% carbon, 0.6 to 0.9% manganese, 0.05% sulfur, and 0.04% phosphor (by weight). RD were installed as side-stream attachments, in parallel with the pipes of the system, under continuous flow at 2 to 3 liters/min and 18 to 20°C. They were positioned downstream and upstream of the NO_3^- dosing point (Fig. 1) to allow direct comparison between the NO_3^--amended (NA) biofilms and the biofilms grown without NO_3^- (control). The pressure levels in the up- and downstream RD were 11×10^5 and 248×10^5 Pa, respectively. The NA and control biofilms were grown over 4 months prior to on-site measurements with microsensors, incubations with $[^{15}N]NO_3^-$ and $[^{35}S]SO_4^{2-}$, and sampling for DNA extraction. After initial sampling, the RD were exchanged; thus NA biofilms no longer received NO_3^- [hereafter, NA(−) biofilms], whereas control biofilms then received NO_3^- [hereafter, control(+) biofilms]. During the 4 days following this exchange, these biofilms [NA(−) and control(+)] were monitored daily to study the biological and biogeochemical responses under changed conditions. Although the target NO_3^- dosage in the injection water for field treatment was 1 mM, dosage irregularities caused NO_3^- levels to vary between 0 and 1.3 mM during the entire trial period. The injection water was filtered (40-μm pore size) and deoxygenated in a Minox system (Minox Technology AS, Norway) (Fig. 1a). Briefly, O_2 was stripped out of the water with N_2 gas, which was subsequently recovered by reacting O_2 with methanol in presence of a catalyst to H_2O, CO_2, and CO. The diffusion of CO_2 into the water phase lowered the pH from pH 8.0 to pH 6.8 to 7.3. Treated water had a salinity of 36‰ (as measured on a refractometer) and contained 27 mM SO_4^{2-}.

Microprofiling. On each of the 4 days after the preincubation period, one biofilm-covered coupon was collected from the RD and placed in a continuous flow cell. Fresh injection water was flushed with argon to remove dissolved oxygen and kept at 18 to 20°C and pH 8.0 (to buffer against acid production); the water was circulated from a medium tank (6 liters) through the flow cells with a velocity of 1 cm s^{-1}. Depth profiles were measured with microsensors for NO_x (sum of NO_3^-, NO_2^-, and N_2O), NO_2^-, N_2O, redox potential (against an Ag/AgCl reference), pH, H_2 (detection limit of 0.1 μM), and H_2S (detection limit of 1 μM) in biofilms amended with 1 mM $NaNO_3^-$ (1, 28, 35, 46, 53). Profiles of H_2S, redox potential, pH, and H_2 were measured in biofilms receiving no NO_3^-. The profiles were recorded using automated profiling software (μ-Profiler; L. Polerecky, Max Planck Institute for Marine Microbiology, Bremen, Germany) in 10- to 25-μm intervals at a vertical angle of 20°. Areal fluxes of NO_3^- and NO_2^- through the diffusive boundary layer were calculated using Fick's first law as described previously (21). Diffusion coefficients used for NO_3^- and NO_2^- in the seawater were 16.1×10^{-6} and 15.3×10^{-6} cm^2 s^{-1}, respectively (37).

^{15}N incubations and analysis. The rates of NO_3^- reduction were measured by ^{15}N stable isotope incubations using $[^{15}N]NO_3^-$ as a tracer, and the ^{15}N products (N_2O, N_2, and NH_4^+) were determined by mass spectrometry. Biofilm coupons were transferred to 6-ml Exetainers (Labco, High Wycombe, Buckinghamshire, United Kingdom), which were then completely filled with NO_3^--free anoxic injection water amended with 485 μM $Na^{15}NO_3$ (98 atom%; Sigma Aldrich, Germany) and 485 μM $Na^{14}NO_3$ in order to obtain maximum sensitivity for the isotope pairing method (45). The Exetainers were sealed, excluding air bubbles. The first set of samples, NA and control(+) biofilms, were incubated for 2.5, 4, 6, 15, 27, and 41 h (Fig. 1). In the second set of incubations, NA(−) and control biofilms were incubated for 7 h after being spiked with NO_3^- label (Fig. 1). Negative controls for each series were prepared and processed in a similar way

as the samples, except that they received fresh coupons without biomass. The incubation was performed at 21 to 23°C in the dark, and bacterial activity was stopped using 1.5 ml of zinc acetate (20%, wt/vol). Rate calculations were based on the initial 7 h of the experiments for the comparison of the two incubation series. Liquid phase $^{14+15}NH_4^+$ was quantified by converting NH_4^+ with hypobromite iodine (69) to N_2 and measured in the same way as N_2 and N_2O. External $^{14+15}NH_4^+$ standards were used for calibration. Gas samples were extracted from a 1-ml helium headspace and injected into a gas chromatograph mass spectrometer (VG Optima, Micromass, United Kingdom) for the N_2 and N_2O isotope composition analysis.

^{35}S tracer incubation and analysis. Exetainers containing single biofilm coupons were filled with in situ water enriched with $[^{35}S]SO_4^{2-}$ tracer (Amersham Bioscience) (final total activity of 100 kBq) and incubated in the dark at room temperature. The incubation was stopped after 2, 4, 6, 12, 24, and 41 h by adding 2 ml of zinc acetate (20%, wt/vol). SO_4^{2-} reduction rate determinations were done using a cold chromium distillation procedure (29), and SO_4^{2-} was quantified by nonsuppressed anion chromatography (Waters 510 pump, Waters IC-Pak anion exchange column, and Waters 430 conductivity detector) (eluent, 1 mM isophthalic acid; flow, 1.0 ml min^{-1}).

Chemical analyses. NO_3^- and NO_2^- from liquid samples were quantified on a chemiluminescence detector (Thermo Environmental Instruments, Franklin, MA) as described previously (6). The dissolved organic carbon (DOC) and organic acid contents of in situ water were quantified by high-temperature combustion using a DOC clone (49) and ion chromatography, respectively.

DAPI staining. After being embedded in 22-oxyacalcitriol cryo-compound (Leica Microsystems GmbH, Wetzlar, Germany), biofilms were removed from the metal surface as a whole block of frozen 22-oxyacalcitriol. Sections 5 μm thick were made using a cryo-microtome (Microm HM 505 E), immobilized on glass slides, and dehydrated in an ethanol series (50, 80, and 96%; 3 min each). DAPI (4′,6′-diamidino-2-phenylindole) was added to each section, and samples were incubated for 10 min in the dark and then examined on a Zeiss Axioplan microscope (Carl Zeiss, Jena, Germany).

Corrosion analyses and S isotope composition. A paraffin-impregnated graphite electrode was used to identify solid iron sulfide compounds in biofilm samples by applying voltammetry of microparticles (48). Following removal of the biofilm (see above), the steel surfaces of coupons from the NA and control biofilms were examined by scanning electron microscopy ([SEM] Hitachi SEM 4004) equipped with energy dispersive X-ray analysis (EDAX PV 9900 UTW). The quantity and stable sulfur (S) isotope composition of the reduced S fraction in the steel coupons (duplicate samples comprised of steel shavings) and from pipeline debris obtained from areas adjacent to the RD receiving no NO_3^- (in triplicates) were determined. The acid-volatile sulfide (AVS) and chromium-reducible sulfur (CRS) fractions were determined by two-step HCl-hot chromous chloride distillations (8). H_2S was trapped as zinc sulfide in 5% zinc acetate solution, and an aliquot of the zinc sulfide suspension was used for sulfide determination according to the method of Cline (9). The remaining zinc sulfide was converted to AgS for stable S isotope analysis. S isotope ratios ($^{34}S/^{32}S$) on the AVS and CRS fractions were analyzed by combustion isotope ratio monitoring mass spectrometry (5). AgS samples were combusted to SO_2 in an elemental analyzer (EuroVector) and introduced into a ThermoElectron Finnigan MAT Delta$^+$ gas mass spectrometer via a ThermoElectron Finnigan MAT Conflo II interface. Stable isotope ratios of $^{34}S/^{32}S$ are given in the δ-notation with respect to the SF_6-based Vienna-Canyon Diablo troilite (V-CDT) standard (11): $\delta^{34}S(‰) = (R_{sample}/R_{V\text{-}CDT} - 1) \times 10^3$, where R is $^{34}S/^{32}S$.

Molecular analysis. Biofilm material for denaturing gradient gel electrophoresis (DGGE) and 16S rRNA gene clone library construction was obtained either from scraping pipelines adjacent to the RD or by flushing the whole RD with sterilized in situ water. Sampling took place after 4 months of growth and again after 4 days of exposure to opposite conditions. All biofilms (biomass of 300 to 500 mg each) were subjected to nucleic acid extraction (bead beating) as described earlier (40). PCR was performed using 50 ng of the DNA extracts in the presence of the bacterial domain-specific primers GM5F (with GC clamp) and 907RC (42). The PCR was run using a hot-start touchdown program to minimize nonspecific amplification. The annealing temperature was decreased from 65 to 55°C every two PCR cycles, after which 12 PCR cycles were performed at 55°C. Equal amounts (1,000 ng) of triplicate PCR products were loaded on the DGGE gel. DGGE was carried out using a Bio-Rad D-Code system run at 60°C at a constant voltage of 200 V for 3.5 h. For cloning, 16S rRNA genes were PCR amplified using the primers GM3F and GM4R (42) at an annealing temperature of 42°C for 30 cycles. PCR products were purified using a QIAquick PCR purification kit (Qiagen, Hilden, Germany), and 200 ng was cloned using a TOPO TA cloning kit (version E; Invitrogen, Karlsruhe, Germany) according to the manufacturer's instructions. Obtained clones were screened by checking their PCR products by gel electrophoresis. The PCR products of the inserts were purified on Sephadex G-50f columns (Amersham Bioscience AB, Uppsala, Sweden) and then sequenced. Sequences were analyzed using ARB software (39) and were inserted into the reconstructed tree by applying parsimony criteria without allowing changes in topology. The number of operational taxonomic units was determined by calculating similarity matrices among the sequences in the ARB database. Sequences with >97% similarity were defined as operational taxonomic units. Rarefaction curves were calculated using the program Analytic Rarefaction (version 1.3, Stratigraphy Lab, University of Georgia; [http://www.uga.edu/~strata/software]). The coverage of the clone libraries, species richness, species evenness, and Shannon-Weaver index of diversity were calculated for each of the four clone libraries, as reported elsewhere (2, 22, 62).

RESULTS

Biofilm morphology and bacterial distribution. The NA and control biofilms grown under in situ conditions for 4 months were visibly different. NA biofilms were fluffy, brownish-yellow, and 150 to 200 μm thick (Fig. 2a). On microscopic examination, the biofilms could be divided into five structurally distinct zones (Fig. 2d and e). DAPI-stained biofilm sections showed that most bacterial cells in the NA biofilms were clustered in a 50-μm-thick horizon near the bottom. This zone was characterized by a sponge-like structure containing voids and channels (Fig. 2d and e, zones 2 and 3). Cells were more sporadically located in a 10-μm-thick crust-like layer directly attached to the metal surface (Fig. 2e, zone 1), while no cells were found in the upper part of the biofilm (Fig. 2e, zones 4 and 5). The control biofilms were ash gray to black, compact, and 50 to 80 μm thick (Fig. 2g), with very low biomass in the 10-μm-thick crust on the metal surface (Fig. 2j and k, zone 1). The biofilms increased in thickness (two to fourfold) during fixation and/or storage (Fig. 2), but the overall structural features were preserved.

Biofilms were then exposed to the opposite growth conditions for 4 days. NA(−) biofilms were found to be visibly patchier than NA biofilms. Zones 4 and 5 disappeared, and cells were evenly distributed across zones 1 to 3. In the control(+) biofilms cells were more abundant in zone 1 than before the NO_3^- addition. Some additional cells also appeared in zone 2 (data not shown).

Spatial distribution of microenvironments and metabolic activity. Microsensor profiles showed clear functional differences among NA and control biofilms (Fig. 3). In the NA biofilms, NO_3^- (0.96 mM in water phase) penetrated throughout the entire biofilm and decreased to 0.86 mM close to the metal surface (Fig. 3a). The nearly linear curve of the NO_3^- profiles inside the biofilm indicated that most NO_3^- consumption occurred in a ~50-μm-thick zone close to the metal surface (at a depth of 150 to 200 μm), i.e., below the maximum depth reached by the microsensor. In this zone, up to 50 μM NO_2^- was produced from the NO_3^-. No clear redox gradients were observed in the NA biofilms, nor was H_2S, H_2, or N_2O detected. In contrast, the control biofilms exhibited strong redox gradients, ranging from 0 mV in the water to −450 mV on the metal surface (Fig. 3b). Nevertheless, neither H_2S, H_2, nor N_2O was detected in these samples either.

After the RD were exchanged, both biofilm types showed metabolic responses within 4 days (Fig. 3c and d). In the NA(−) biofilms, the redox potential initially decreased from 0 to −330 mV near the metal surface within the first 24 h and

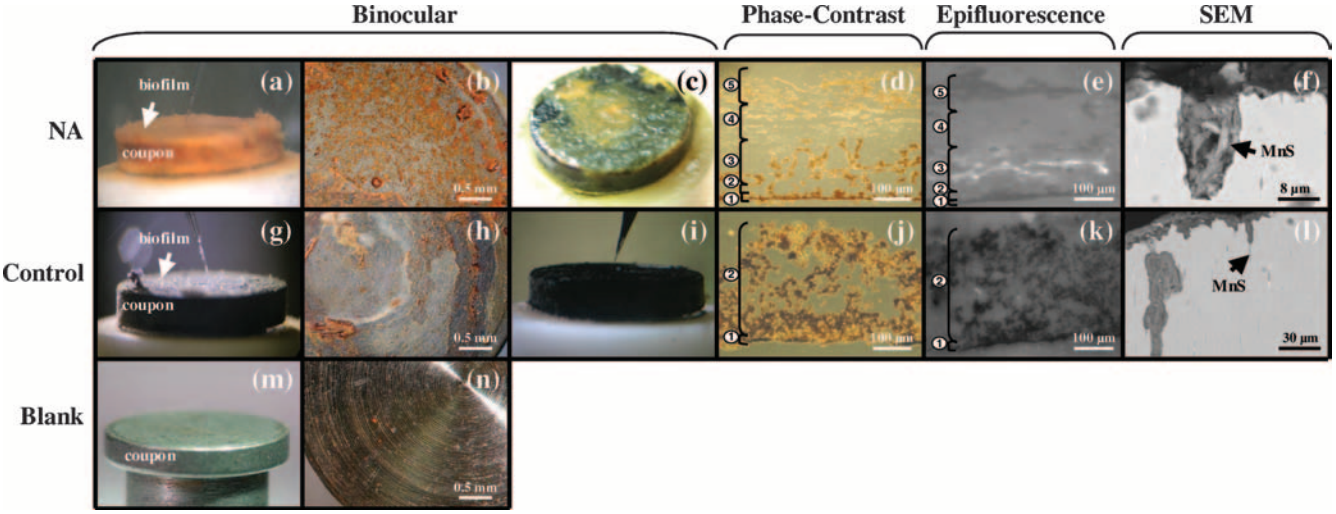

FIG. 2. NA (a to f) and control (g to l) biofilms visualized by different approaches. Fresh coupons are shown in panels m and n. Binocular images show complete carbon steel coupons before (a and g) and after (b and h) removal of biofilm cover and after exposure of biofilms to sulfide (c and i). The phase-contrast microscopy images of 5-μm-thick biofilm cross-sections show structurally distinct zones, indicated by the numbers (d and j). Epifluorescence microscopy was applied to the cross-sections from the phase-contrast microscopy (e and k). Positive DAPI signals appear in white. SEM (backscattered electron) images show vertical coupon cross-sections. The arrows indicate MnS inclusions associated with pits (l) and surrounded by organic material inside pits (f).

then stabilized at −215 mV (Fig. 4). In the control(+) biofilms, NO_3^- uptake started 24 h after the NO_3^- addition. Most of the NO_3^- was converted to NO_2^-, again, in a ~30-μm-thick layer close to the metal surface (Fig. 3d and Table 1). In the control(+) biofilm the redox potential on the metal surface increased from −450 to −270 mV over 96 h (Fig. 3d and 4). Net NO_3^- fluxes in NA and control(+) biofilms were almost equal, whereas the NO_2^- flux in control(+) biofilms was three times higher than in NA biofilms (Table 1). All biofilms were anoxic during the measurements, as assessed by an oxygen microelectrode (52).

During the 4-month growth period, the total DOC content in the water column ranged between 2 and 50 mg liter^{-1}, and concentrations of the volatile fatty acids formate, acetate, propionate, and butyrate were below 0.1 mg liter^{-1}. The potential for denitrification under such oligotrophic conditions was assessed on an NO_3^--amended (1 mM) NA biofilm using an N_2O microsensor and the acetylene block method (54). While no N_2O was formed in the absence of methanol, the N_2O level near the metal surface increased within the following 37 min after the addition of methanol as a carbon source (1 mM) (Fig. 5). This indicated that the electron donor supply ordinarily limits the denitrification in the system.

N and S conversion rates. The NO_3^- reduction products and N conversion rates in the biofilms were determined from ^{15}N incubations (Table 1). The highest NO_3^- reduction rate among all incubations was measured in NA biofilms. Consistent with the microprofiling results, NO_2^- was the main intermediate product from NO_3^- reduction in NA biofilms, with N_2 and NH_4^+ as end products. NO_3^- added to control biofilms (necessary for the determination of potential NO_3^-reduction rates) was solely converted to NH_4^+, suggesting DNRA.

During the opposite experiment, NA(−) biofilms receiving NO_3^- after a 4-day exposure to NO_3^--free conditions still reduced NO_3^- to NO_2^-, N_2, and NH_4^+ at rates comparable to NA biofilms (Table 1). In the control(+) biofilms, the same nitrogen products as in NA biofilms were formed but at lower rates. As the level of N_2 constantly increased after 24 h of ^{15}N incubation in control(+) biofilms (data not shown), this suggests denitrification. Net fluxes of NO_3^- and NO_2^- in NA and control(+) biofilms calculated from microprofiles were generally higher than rates determined by ^{15}N measurements, presumably due to mass transfer limitations during the isotope incubations and to heterogeneity between the biofilms.

The SO_4^{2-} reduction rates in all biofilms were below the detection limit of the radiotracer method of 38 pmol of SO_4^{2-} cm^{-3} day^{-1}, as determined according to the method of Kallmeyer et al. (29).

Effect of NO_3^- on bacterial diversity. DGGE and 16S rRNA gene cloning showed distinct differences in microbial communities within the two biofilms, with higher species richness (number of bands) in the control than in the NA biofilms (Fig. 6, left panels). After the conditions were changed, within 4 days both techniques showed insignificant community changes in the NA(−) biofilms, but the diversity in control(+) biofilms had declined (Fig. 6, right panels). In NA biofilms under NO_3^- and NO_3^--free conditions, all sequences belonged to the *Gammaproteobacteria*, and the highest number of obtained sequences were closely related to *Methylophaga* spp., uncultured environmental clones obtained from Arctic pack ice (7), and *Colwellia* spp. (see Fig. S2 in the supplemental material). The community structure of the control biofilms was comprised of different proteobacterial sequences (alpha, gamma, delta, and epsilon subgroups) as well as those related to the *Cytophaga-Flavobacteria-Bacteriodetes* group. The vast majority (80%) of obtained sequences was related to the gammaproteobacterial Arctic pack ice clones (7) (see Fig. S3 in the supplemental material). Following NO_3^- addition, the percentage of sequences within the clone library compiled from control(+) biofilms shifted in favor of *Methylophaga*- and *Colwellia*-related

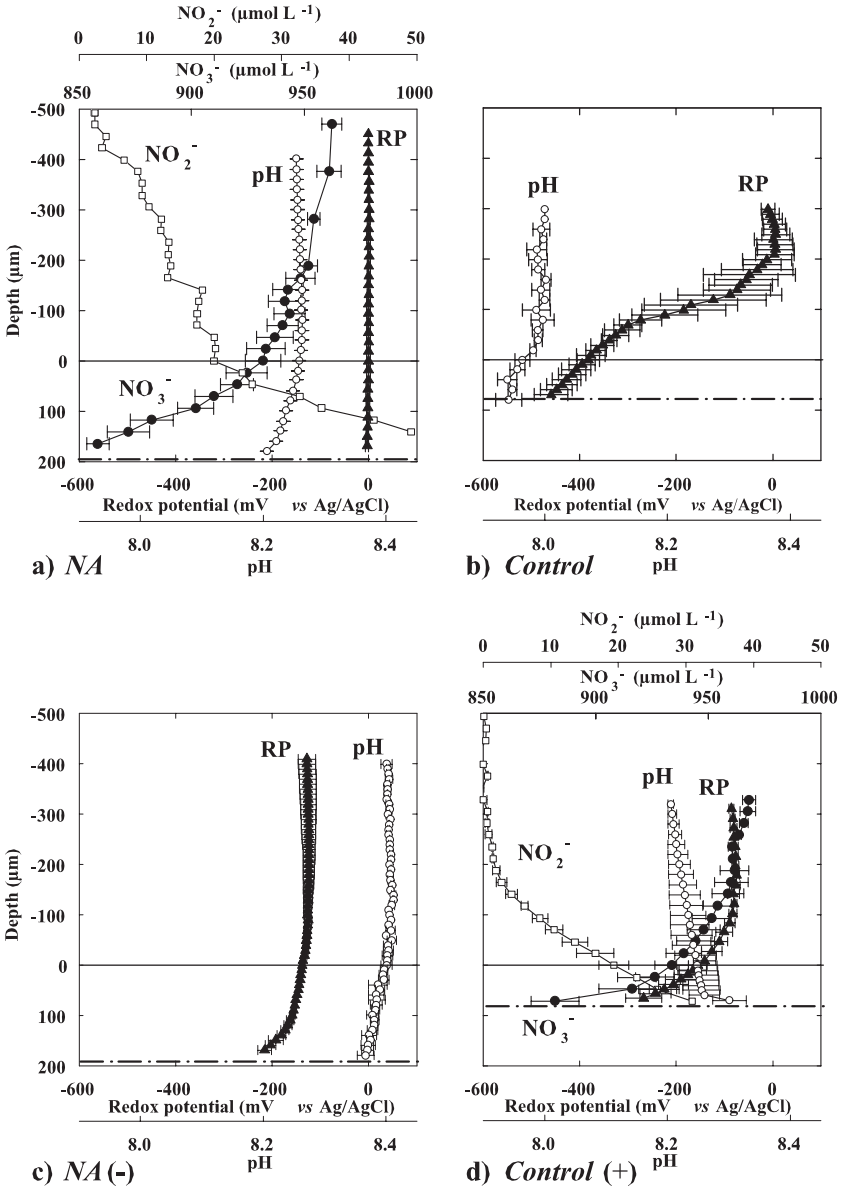

FIG. 3. (a and b) Microprofiles of NO_3^-, NO_2^-, redox potential (RP), and pH in NA and control biofilms grown in situ on carbon steel coupons for 4 months. (c and d) The situation 4 days after biofilm exchange to opposite NO_3^- conditions, designated NA(−) and control(+) biofilms. H_2S, H_2, and N_2O were not detected in any biofilm. Zero depth indicates the biofilm-water boundary; dashed lines represent the estimated metal coupon surface position. Averages and standard deviations were calculated from three profiles measured across the biofilm.

sequences (together, 76%), while the percentage of sequences related to the Arctic pack ice clones was reduced from 80 to 22% (Fig. 6, right). The coverage within the four clone libraries was 81 to 93% (see Fig. S1 and Table S1 in the supplemental material).

Corrosion analysis. The matrix of control biofilms contained greigite (Fe_3S_4) while no known iron corrosion product was detected in the matrix of NA biofilms. The surface of newly manufactured coupons showed grinding marks (Fig. 2n), which disappeared from the surface under the control biofilms, indicating uniform corrosion (Fig. 2h). Conversely, the grinding marks were still intact under NA biofilms (Fig. 2b), indicating mitigation of uniform corrosion by NO_3^-. However, SEM imaging of vertical coupon cross-sections revealed the presence of irregularly shaped, deep (up to 200 μm) pits underneath both types of biofilms (Fig. 2f and l). These pits were not present in newly manufactured coupons. Pits were often narrow and deep troughs, but laterally running subsurface pits were also found. SEM-energy dispersive X-ray analysis showed that biofilm residues on all coupon surfaces were enriched in iron ions and oxides, but only control biofilms contained iron sulfides. Embedded in the steel matrix orthogonal to the surface, needle-shaped manganese sulfide (MnS) inclusions were often associated with pits (one example is shown in Fig. 2f and l). The MnS inclusions were surrounded by an amorphous matrix, rich in the elements carbon, iron, oxygen, phosphor,

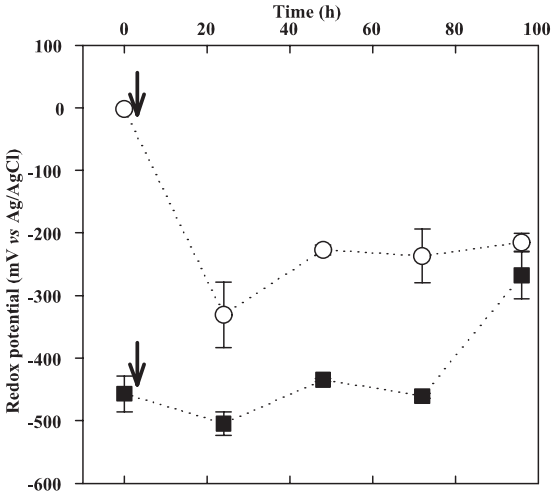

FIG. 4. Redox potential dynamics on the coupon surface in NA (○) and control (■) biofilms during the 4-day tests. Arrows indicate the time of NO_3^- removal from NA biofilms and the addition of NO_3^- to control biofilms. Averages and standard deviations from three values measured at spots across the metal surface are shown.

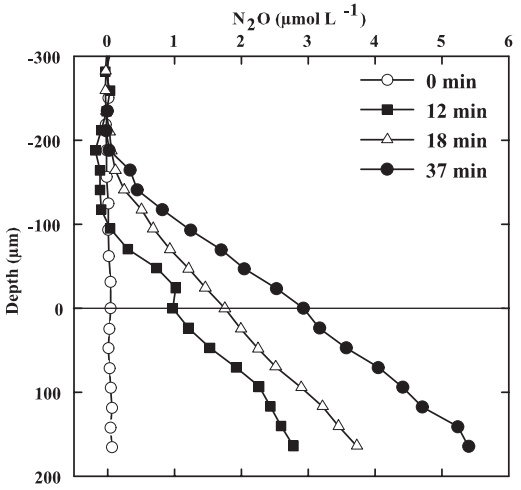

FIG. 5. Test of carbon limitation as measured by N_2O production in an NA biofilm using an N_2O microsensor and applying the acetylene block technique. Data represent N_2O formation before (0 min) and after (12, 18, and 37 min) the addition of 1 mM methanol in the presence of 1 mM NO_3^-.

and sulfur (Fig. 2f), which is characteristic for organic matter. Sulfur as AVS from the MnS particles was determined to account for 0.27 ± 0.00 weight percent of the steel and had a $\delta^{34}S_{AVS}$ of +1.54 ‰ ± 0.04‰. In the pipeline debris, AVS and CRS made up ca. 0.1 and 0.8 weight percent of the total sulfur (S_{total}) with $\delta^{34}S_{AVS}$ of −9.73 ‰ ± 0.05‰ and $\delta^{34}S_{CRS}$ of −15.28 ‰ ± 0.21‰, respectively.

DISCUSSION

Spatial distribution of microenvironments and metabolic activity. For the first time, the spatial distribution of bacteria and their metabolic activities within biofilms from a water injection system for oil recovery have been described in situ with minimal disturbance of the biofilm structure. The spatial distributions of metabolic processes and cell densities within the biofilms correlate well (Fig. 2 and 3). The biofilms were heterogeneous in structure, and most of the N conversions occurred in a narrow ~30- to 50-μm-thick zone at the biofilm base. Upon addition to the biofilms, NO_3^- penetrated the biofilm through to the metal surface, where it was mainly converted to NO_2^-. The NO_2^- was partly further reduced to N_2 and NH_4^+, as revealed by ^{15}N labeling (Table 1) and partly diffused out of the biofilm (Fig. 3a and d). The open structure of the biofilms may facilitate mass transfer of nutrients and electron donors from the overlaying water down to the metal surface, where most bacterial cells were found. Here, alternative sources of electron donors for NO_3^- reduction and for other reductive biotransformations might have been anodic iron and cathodic hydrogen from the corroding steel (12, 68).

Redox potential measurements clearly showed that all NO_3^--treated biofilms exhibited fewer negative values than those biofilms without NO_3^-. It is evident that the NO_3^- treatment drastically affected the dominant metabolic processes in the biofilms. It should be mentioned that the platinum microsensor used to measure the oxidation reduction potential status in the biofilms does not respond to all redox couples but primarily to Fe^{2+}, sulfide, and H_2. Notably, the sensor does not respond to NO_3^- or NO_2^- and responds very slowly to oxygen. Furthermore, it is important to note that the different redox couples in a solution are rarely in equilibrium (63). For example, dissolved NO_3^- does not chemically react with H_2S; thus, a mixture of both is stable in the absence of a catalyst. In the absence of electroactive species, the redox signal will not sta-

TABLE 1. N fluxes calculated from microprofiles and ^{15}N isotope measurements

Condition and biofilm type[a]	Microsensor flux (n)[b]		Conversion rate with ^{15}N incubation (n = 1)[b]					
	NO_3^-	NO_2^-	$^{14+15}NO_3^-$	$^{14+15}NO_2^-$	$^{29+30}N_2$	$^{29+30}N_2O$	$^{15}NH_4^+$	Recovery (%)
Before exchange (4 mo)								
NA	−16.6 ± 2.4 (3)	5.4 (1)	−6.02	4.97	0.44	0.00	0.35	96
Control^{spike}	—	—	−0.35	0.08	0.00	0.00	0.26	98
After exchange (4 days)								
NA(−)^{spike}	—	—	−4.68	4.17	0.25	0.01	0.20	99
Control(+)	−22.5 ± 2.6 (3)	14.0 ± 2.3 (2)	−2.12	1.24	0.01	0.00	0.83	98

[a] Spike, biofilms previously incubated without NO_3^- (4 months or 4 days, as indicated) and then dosed with $^{14+15}NO_3^-$.
[b] Values are μmol of N cm^{-2} day^{-1}. n, number of replicate measurements; —, not measured.

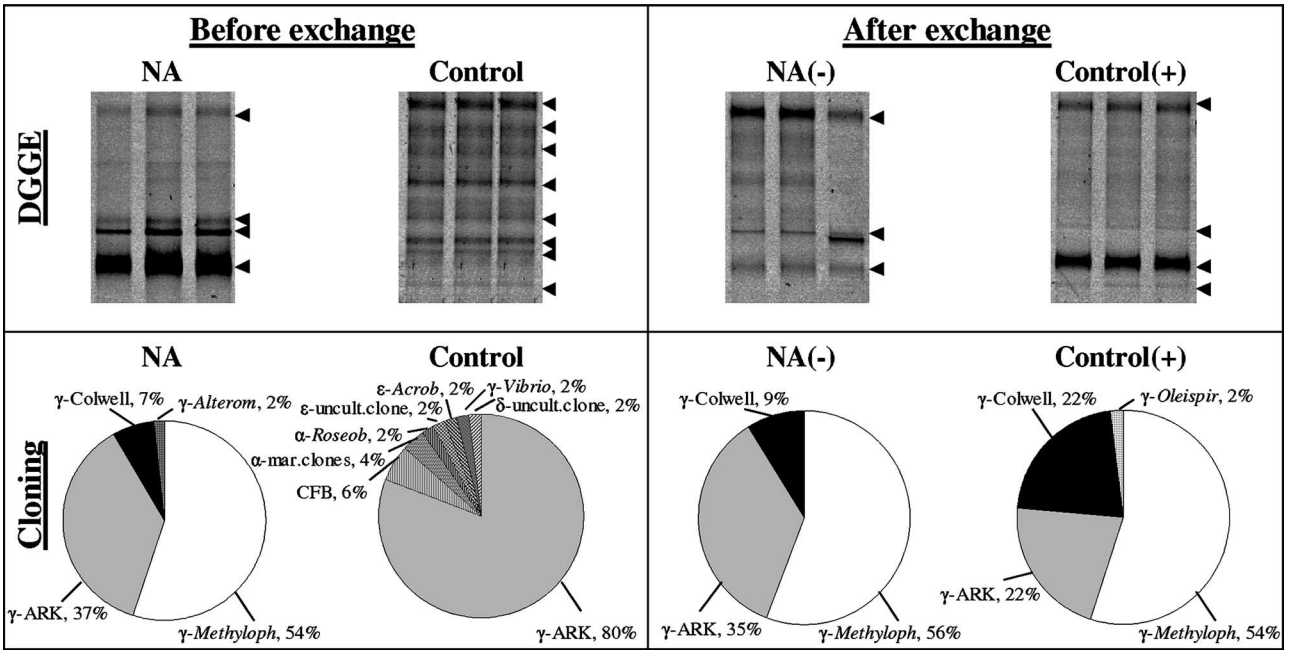

FIG. 6. (Top) DGGE fingerprints (in triplicate) of PCR-amplified 16S rRNA gene fragments obtained from NA and control biofilms before (4 months) and after (4 days) exchange using bacterial primers GM5F and 907RC. Arrows indicate the visible dominant bands. (Bottom) 16S rRNA gene cloning showing differences in the bacterial community composition in NA and control biofilms before and after exchange to opposite NO_3^- conditions. The relative abundance (percent) of sequences in each clone library (i.e., treatment) with the closest relative and the taxonomic affiliation is given. α, *Alphaproteobacteria*; γ, *Gammaproteobacteria*; δ, *Deltabateria*; ε, *Epsilonbacteria*; Alterom, *Alteromonas* sp.; *Arcob*, *Arcobacter* sp.; ARK, environmental Artic pack ice clones; CFB, *Cytophaga*/*Flavobacteria*/*Bacteriodes*; Colwell, *Colwellia* sp.; *Methyloph*, *Methylophaga* sp.; *Roseob*, *Roseobacter* sp.; *Oleispir*, *Oleispira* sp.; uncult, uncultured; mar, marine.

bilize, as it does in the anoxic water phase and the boundary layer. Near the metal surface, however, stable, reproducible readings indicated the presence of electroactive compounds (Fig. 3 and 4). The signal near the metal surface increased upon the NO_3^- addition to the control biofilms, but since the sensor does not respond directly to NO_3^-, this increase was caused by an NO_3^--induced decrease in the concentrations of electroactive compounds such as Fe^{2+}, S^{2-}, or H_2 (36). As free H_2S and H_2 were not detected, dissolved Fe^{2+} is probably the main determinant for the redox signal and is suggestive of Fe corrosion. The decrease in redox potential after the removal of NO_3^- in NA biofilms can be explained by both enhanced Fe^{2+} release from the steel surface and decreased oxidation of Fe^{2+} (Fig. 4). The former process must have been significant in the case of the control coupons that showed substantial surface loss. Conclusive evidence on corrosion can be obtained from the redox potential and SEM data. Interpreted with care and in combination with other methods, the redox microsensor is a useful tool to detect and localize both the effect of treatment and/or MIC processes under in situ anoxic conditions.

Impact of NO_3^- on biofilm communities. The presence of NO_3^- led to greatly increased rates of biomass growth and respiratory activity (NO_3^- reduction). Rates of NO_3^- reduction and turnover were several orders of magnitude higher than SO_4^{2-} reduction in the control samples, the latter being below the detection limit of the radiotracer method (i.e., 38 pmol of SO_4^{2-} cm^{-3} day^{-1}). Indicators of dissimilatory SO_4^{2-} reduction in the control samples were nearly nonexistent: there was no free H_2S, SO_4^{2-} reduction rates were undetectable with sensitive radiotracer techniques, and known SRB were not found (except for a single gammaproteobaterial clone) (Fig. 6), although the latter were previously detected in biofilm debris obtained at the end of the same 9-km-long injection pipeline (34). The finding of Fe_3S_4 together with the background SO_4^{2-} reduction rates measured here and the low abundance of SRB in our control biofilm samples, as opposed to their previous detection (34), are indicative of variable temporal abundance and/or activity of SRB within the system. With regard to MIC, it should be noted that the number of bacteria, either attached or planktonic, does not necessarily correlate with the extent of corrosion; the latter is considered to be linked to metabolic cell activity (reference 3 and references cited therein).

The addition of NO_3^- led to a shift from a low-biomass but species-rich community to a high-biomass NO_3^--reducing community with low diversity. This effect of NO_3^- on the bacterial community structure and diversity can most plausibly be explained by interspecies competition and direct inhibition by NO_2^-, as was previously suggested (25, 27, 50, 60). In the presence of NO_3^-, domination by NRB of indigenous control biofilm populations occurred due to the competition for limited electron donors under the prevailing oligotrophic conditions although total DOC concentrations could occasionally peak (up to 50 mg/liter), e.g., during algal blooms in the sea. Possible electron donors in the system were methanol, formaldehyde, formate, CO_2, and CO that derive from the complete and incomplete deoxygenation reaction with methanol and can be carried over from the deoxygenation system into the injection water (Fig. 1a). Other possible electron donors

were organic carbon from decaying algal biomass, sulfide, Fe^0, and H_2. NO_3^- reduction is thermodynamically more favorable than SO_4^{2-} reduction and has a higher biomass yield (72). Populations able to denitrify can therefore rapidly become dominant and efficiently consume the electron donor. The inhibition by NO_2^- can well lead to a community shift. It is a strong inhibitor of the sulfite reductase and thus inhibits SRB activity, as was previously shown in field and laboratory applications (26, 32, 43, 44, 50). NO_2^- levels of 0.05 mM (Fig. 3) at the base of the biofilms may have contributed to the change in community composition. It cannot be concluded here which specific bacterial group that appeared after the addition of NO_3^- to control biofilms was responsible for the NO_2^- production. Strains of *Methylophaga* (strictly aerobic methylotrophs), *Colwellia* (facultative anaerobic chemoheterotrophs), and *Oleispira* (facultative anaerobic chemoheterotrophs) have all been reported to reduce NO_3^- to NO_2^- (13, 47, 70, 71). *Colwellia*-related bacteria may have reduced the NO_2^- partly to N_2, as was reported for cultures of *Colwellia maris* (47).

NO_3^- added to control biofilms was converted to NH_4^+ via NO_2^- as an intermediate. NH_4^+ was potentially formed either by the indigenous populations through DNRA or abiotically, i.e., by the reaction of NO_3^-/NO_2^- with metallic iron (32). However, the increased production of NH_4^+ during the ^{15}N incubation relative to the negative control indicated that NH_4^+ formation was biogenic. Candidates capable of DNRA in the control biofilms were fermentative *Vibrio* spp. (31, 67). DNRA is energetically favorable under conditions of electron acceptor limitation (low levels of NO_3^-/NO_2^- relative to the electron donor) and yields energy ($\Delta G'^0$ of -679.61 kJ mol^{-1}). It is also considered a detoxification pathway for NO_2^- in organisms containing an NO_2^- reductase (23, 67). DNRA might have protected indigenous populations from immediate NO_2^- inhibition in the control biofilms. However, the prolonged addition (4 days) of NO_3^- to these biofilms led to a rapid decrease in diversity, probably because NRB populations (*r* strategists) (30) grew faster than indigenous populations (*K* strategists). Furthermore, the relative decrease of the indigenous population could be due to the enhanced formation by NRB of NO_2^- that cannot be detoxified anymore via DNRA.

Conversely, the removal of NO_3^- from the NA biofilms resulted neither in a community shift nor in a decrease in potential NO_3^- reduction. Even after 4 days without NO_3^-, upon the readdition of NO_3^-, it was instantly reduced. The period of absence of NO_3^- was likely too short for the NRB populations to disappear and the typical control biofilm community to establish. This is favorable for the operation of the injection water system as fluctuations in the NO_3^- concentrations caused by shutdowns in NO_3^- dosing or maintenance work, for example, will not lead into instant growth of SRB. However, this stability in the community composition is not coupled to a functional stability; i.e., the redox potential does decrease within days upon NO_3^- removal (Fig. 4). Therefore, a continuous addition of NO_3^- might be preferred to prevent corrosion.

Sources and sinks of H_2S. Microsensor, molecular, and tracer methods all suggest that the dissimilatory SO_4^{2-} reduction occurred at low rates in the control biofilms. However, metal sulfides made up part of the crust found both on the coupons and in debris collected from a pipeline adjunct to the RD. The H_2S produced might have reacted quickly with iron ions embedded in the biofilm matrix to form black iron sulfide precipitates, thereby preventing its detection. Indeed, ~140 μM sulfide experimentally added to the water phase above coupons instantly resulted in FeS precipitation (Fig. 2c and i), and the sulfide concentrations inside the biofilms remained below the detection level (data not shown). The finding of Fe_3S_4 exclusively in the control biofilms also provides indirect evidence for the formation of H_2S. This H_2S must have derived from either (i) dissimilatory reduction of SO_4^{2-} by SRB, occurring at very low rates or episodically; (ii) bacterial degradation of S-containing amino acids (e.g., from algae, seawater organic particles, or the biofilm itself [14]); or (iii) biotic or abiotic dissolution of sulfide from S-containing inclusions embedded in the steel matrix (details below). The stable S isotope composition ($^{34}S/^{32}S$) of the sulfides in pipeline debris indicates that bacterial SO_4^{2-}reduction has occurred. Dissimilatory SO_4^{2-} reduction and the associated isotope fractionation are the only processes that could lead to the depleted values observed in the debris, i.e., $\delta^{34}S_{AVS}$ of -9.73 ‰ ± 0.05‰ and $\delta^{34}S_{CRS}$ of -15.28 ‰ ± 0.21‰. The sulfide derived from the MnS inclusions or biosynthetic sulfur alone would have an S isotope composition of close to +1.5‰ or +18‰, respectively. Conversely, the sulfide in the debris was depleted in ^{34}S relative to both seawater SO_4^{2-} (+20‰) and the MnS (+1.5‰). While some of the sulfide may derive from MnS dissolution of steel inclusions, the depleted S in the sulfide crust is consistent with the low rates of background SO_4^{2-} reduction and consequent sulfide production in the injector.

Corrosion damage. NO_3^- injection into reservoirs for souring control may prevent or mitigate the risks from MIC within the injection pipelines (38, 66). However, corrosion occurred on the coupon surfaces underneath both NA and control biofilms and so was not entirely prevented by the NO_3^- treatment, although its addition did change the type and extent of corrosion. NA biofilm coupons were less affected by uniform corrosion than the control coupons due to the inhibition of sulfide production. The variation in corrosion patterns between NA and control biofilms can be explained by the nature of the biofilms and their distribution over the metal surface. Biofilms are well known to affect the electrochemistry of the near-surface milieu as they modify the physicochemical environment within which the corrosion reactions occur (58). Matrix-bound Fe^{2+} and Fe^{3+} are thought to shuttle electrons from the steel to a suitable electron acceptor such as NO_3^-, NO_2^-, and O_2, leading to differential corrosion cells that accelerate corrosion (4). It was estimated for control biofilm coupons that 2% of the S_{total} from the steel matrix (which contained 535 μmol of S_{total} cm^{-3}) could dissolve during the pitting process. This released sulfide could contribute up to 11% of the S_{total} in the biofilm crust.

The NO_3^- treatment did not protect against pitting corrosion and may have even accelerated it via the chemical oxidation of metallic iron with NO_3^-/NO_2^- with consequent reduction to NH_4^+ (32, 51, 68). Indeed, NO_2^- concentrations of 30 and 50 μM at the metal surface in the biofilms (Fig. 3) are in the range where NO_2^- is reported to be corrosive (<3.5 mM) (reference 26 and references cited therein). Nevertheless, NO_3^- is used to inhibit SRB activity in seawater oil recovery

systems, with one of the intentions being to reduce MIC pitting. We cannot deduce from the data to what extent either of these processes contributed to the pitting on NO_3^--amended coupons; however, it is evident that the NO_3^- addition strongly reduced the uniform surface corrosion.

Many pits on the corroded coupons were closely associated with needle-shaped MnS inclusions embedded in the steel matrix (Fig. 2f and l). Notably, this was independent of the NO_3^- treatment. MnS inclusions are ordinarily formed from manganese and sulfur additions to the steel during its manufacturing. Dissolving inclusions are known to increase the susceptibility of steel to electrochemical pit formation (reference 59 and references cited therein). In addition, bacteria seem involved in the initiation and propagation of pitting at these particles (10). The association of organic matter and MnS inclusions in the coupons implies that the pit formation was indeed microbially influenced. MnS inclusions dissolve into Mn^{2+} and H_2S at a pH and redox potential below 4.8 and −100 mV, respectively (17). The pH in the injection water was 6.8 to 7.3; thus, a pH gradient of at least two units over a distance of up to 400 μm is needed to obtain a pH at the bottom of the pits of below 4.8. Such steep pH gradients were earlier found and were attributed to the formation of protons from the hydrolysis by Fe^{2+} and the formation of hydroxides (32, 36). We suggest that released Mn^{2+} and H_2S from MnS inclusions may serve as precursors for biochemical manganese and sulfur cycles in the biofilms. In the absence of NO_3^-, the dissolved H_2S might further react with iron to form greigite (Fe_3S_4) inside the biofilm at close to neutral pH values. The overall reaction of MnS dissolution and Fe_3S_4 formation from metal iron is thermodynamically favorable under standard conditions and pH 7 and is proposed to proceed as follows: $4MnS(s) + 3Fe^0(s) + 8H^+(aq) \rightarrow Fe_3S_4(s) + 4Mn^{2+}(aq) + 4H_2(aq)$, where $\Delta G'^0$ is -32.86 kJ mol^{-1}.

The removal of cathodic H_2 by bacteria and the oxidation of Mn^{2+} with tracers of oxygen from the reaction accelerate the consumption of metal iron and the production of Fe_3S_4, thus enhancing corrosion. Under in situ conditions, the energy gain from this reaction is supposed to be even higher. Greigite is a metastable iron sulfur compound formed at low pH from preexisting mackinawite (FeS) by biogenic aldehydic carbonyls (55, 56). As it is only stable at pH values between 5.5 and 7.0 in a range of redox potential between −200 and 400 mV (56), the exclusive detection of Fe_3S_4 inside the control biofilms is indicative of its formation inside the biofilm. Whether the MnS dissolution and Fe_3S_4 formation are mediated by microbes and coupled to iron oxidation to produce energy is interesting and needs further investigation.

Summary and conclusions. Our combined results provide the first insights into complex metal-microbe interactions under in situ conditions and show that NO_3^- amendments strongly induced structural and functional changes in the marine biofilms. NO_3^- addition led to a shift from a low, but species-rich, biomass to a high-biomass, NO_3^--reducing community with low diversity. Rates of NO_3^- reduction and turnover were several orders of magnitude higher than dissimilatory SO_4^{2-} reduction. Greigite, exclusively detected in the control biofilms, provides evidence that SO_4^{2-} reduction occurred either at low rates or episodically. Corrosion analyses revealed that uniform corrosion was microbially influenced, while this was less clear for pitting corrosion. Whereas pitting corrosion was not affected by the treatment, uniform corrosion was mitigated by the addition of NO_3^-. MnS inclusions embedded in the steel matrix may play an important role in the pitting process. It is proposed that bacteria might be involved in their dissolution and combine this with the oxidation of metal iron to gain energy in the absence of NO_3^-.

ACKNOWLEDGMENTS

We thank G. Eickert, I. Schoeder, K. Hohmann, and C. Wiegand for microsensor construction. K. Kohls (MPI Bremen) and H. Juling (Bremen Institute for Materials Testing) are acknowledged for assistance with ARB and SEM imaging, respectively. C. Hubert and L. Polerecky (both at MPI Bremen) are thanked for comments on an earlier version of the manuscript. We are grateful to Jan Larsen (Maersk Oil og Gas, Denmark), who provided access to the sampling site. We thank two anonymous reviewers for useful suggestions on the manuscript.

This work was supported by the Max Planck Society, Germany, and by Oil Plus Ltd., Berkshire, United Kingdom.

REFERENCES

1. **Andersen, K., T. Kjær, and N. P. Revsbech.** 2001. An oxygen insensitive microsensor for nitrous oxide. Sens. Actuators B **81:**42–48.
2. **Atlas, R. M., and R. Bartha.** 1998. Microbial ecology: fundamental and application. Benjyamin/Cummings Science Publishing, Menlo Park, CA.
3. **Beech, I. B., and C. C. Gaylarde.** 1999. Recent advances in the study of biocorrosion—an overview. Rev. Microbiol. **30:**177–190.
4. **Beech, I. B., and J. Sunner.** 2004. Biocorrosion: towards understanding interactions between biofilms and metals. Curr. Opin. Biotechnol. **15:**181–186.
5. **Boettcher, M. E., and B. Schnetger.** 2004. Direct measurement of the content and isotopic composition of sulfur in black shales by means of combustion-isotope-ratio-monitoring mass spectrometry (C-irmMS), p. 597–603. *In* P. A. de Groot (ed.), Handbook of stable isotope analytical techniques. Elsevier, Amsterdam, The Netherlands.
6. **Braman, R. S., and S. A. Hendrix.** 1989. Nanogram nitrite and nitrate determination in environmental and biological materials by vanadium(III) reduction with chemiluminescence detection. Anal. Chem. **61:**2715–2718.
7. **Brinkmeyer, R., K. Knittel, J. Jurgens, H. Weyland, R. Amann, and E. Helmke.** 2003. Diversity and structure of bacterial communities in Arctic versus Antarctic pack ice. Appl. Environ. Microbiol. **69:**6610–6619.
8. **Canfield, D. E., R. Raiswell, J. T. Westrich, C. M. Reaves, and R. A. Berner.** 1986. The use of chromium reduction in the analysis of reduced inorganic sulfur in sediments and shales. Chem. Geol. **54:**149–155.
9. **Cline, J. D.** 1969. Spectrophotometric determination of hydrogen sulfide in natural waters. Limnol. Oceanogr. **14:**454–&.
10. **Crolet, J.-L.** 2005. Microbial corrosion in the oil industry: a corrosionist's view, p. 143–169. *In* O. Bernard and M. Magot (ed.), Petroleum microbiology. ASM Press, Washington, DC.
11. **Ding, T., R. Bai, Y. Li, D. Wan, X. Zou, and Q. Zhang.** 1999. Determination of the absolute $^{32}S/^{34}S$ ratio of IAEA-S-1 reference material and V-CDT sulfur isotope standard. Sci. China D **42:**45–51.
12. **Dinh, H. T., J. Kuever, M. Mussmann, A. W. Hassel, M. Stratmann, and F. Widdel.** 2004. Iron corrosion by novel anaerobic microorganisms. Nature **427:**829–832.
13. **Doronina, N. V., T. D. Lee, E. G. Ivanova, and Y. A. Trotsenko.** 2005. *Methylophaga murata* sp. nov.: a haloalkaliphilic aerobic methylotroph from deteriorating marble. Microbiology **74:**440–447.
14. **Duan, J. Z., B. R. Hou, and Z. G. Yu.** 2006. Characteristics of sulfide corrosion products on 316L stainless steel surfaces in the presence of sulfate-reducing bacteria. Mater. Sci. Eng. C **26:**624–629.
15. **Eckford, R. E., and P. M. Fedorak.** 2002. Chemical and microbiological changes in laboratory incubations of nitrate amendment "sour" produced waters from three western Canadian oil fields. J. Ind. Microbiol. Biotechnol. **29:**243–254.
16. **Eckford, R. E., and P. M. Fedorak.** 2004. Using nitrate to control microbially-produced hydrogen sulfide in oil field waters, p. 307–340. *In* R. Vazquez Duhalt and R. Quintero-Ramirez (ed.), Petroleum biotechnology: developments and perspectives, vol. 151. Elsevier Science Bv, Amsterdam, The Netherlands.
17. **Eklund, G. S.** 1974. Initiation of pitting at sulfide inclusions in stainless steel. J. Electrochem. Soc. **121:**467–473.
18. **Evans, L. V.** 2000. Biofilms: recent advances in their study and control. Harwood Academic Publishers, Amsterdam, The Netherlands.

19. **Gardner, L. R., and P. S. Stewart.** 2002. Action of glutaraldehyde and nitrite against sulfate-reducing bacterial biofilms. J. Ind. Microbiol. Biotechnol. **29:**354–360.
20. **Geesey, G. G., and J. D. Bryers.** 2000. Biofouling of engineered materials and systems, p. 237–279. *In* J. D. Bryers (ed.), Biofilms II: process analysis and applications. Wiley-Liss, Inc., New York, NY.
21. **Gieseke, A., and D. de Beer.** 2004. Use of microelectrodes to measure *in situ* microbial activities in biofilms, sediments, and microbial mats, p. 1581–1612. *In* G. G. Kowalchuk, F. J. de Bruijn, I. M. Head, A. D. Akkermans, and J. D. van Elsas (ed.), Molecular microbial ecology manual, 2nd ed. Springer, Heidelberg, Germany.
22. **Good, I. J.** 1953. The population frequencies of species and the estimation of population parameters. Biometrika **40:**237–264.
23. **Greene, E. A., C. Hubert, M. Nemati, G. E. Jenneman, and G. Voordouw.** 2003. Nitrite reductase activity of sulphate-reducing bacteria prevents their inhibition by nitrate-reducing, sulphide-oxidizing bacteria. Environ. Microbiol. **5:**607–617.
24. **Hall-Stoodley, L., J. W. Costerton, and P. Stoodley.** 2004. Bacterial biofilms: from the natural environment to infectious diseases. Nat. Rev. Microbiol. **2:**95–108.
25. **Haveman, S. A., E. A. Greene, C. P. Stilwell, J. K. Voordouw, and G. Voordouw.** 2004. Physiological and gene expression analysis of inhibition of *Desulfovibrio vulgaris* Hildenborough by nitrite. J. Bacteriol. **186:**7944–7950.
26. **Hubert, C., M. Nemati, G. Jenneman, and G. Voordouw.** 2005. Corrosion risk associated with microbial souring control using nitrate or nitrite. Appl. Microbiol. Biotechnol. **68:**272–282.
27. **Hubert, C., and G. Voordouw.** 2007. Oil field souring control by nitrate-reducing *Sulfurospirillum* spp. that outcompete sulfate-reducing bacteria for organic electron donors. Appl. Environ. Microbiol. **73:**2644–2652.
28. **Jeroschewski, P., C. Steuckart, and M. Kuhl.** 1996. An amperometric microsensor for the determination of H_2S in aquatic environments. Anal. Chem. **68:**4351–4357.
29. **Kallmeyer, J., T. G. Ferdelman, A. Weber, H. Fossing, and B. B. Jørgensen.** 2004. A cold chromium distillation procedure for radiolabeled sulfide applied to sulfate reduction measurements. Limnol. Oceanogr. Methods **2:**171–180.
30. **Kassen, R., and P. B. Rainey.** 2004. The ecology and genetics of microbial diversity. Annu. Rev. Microbiol. **58:**207–231.
31. **Kelso, B. H. L., R. V. Smith, R. J. Laughlin, and S. D. Lennox.** 1997. Dissimilatory nitrate reduction in anaerobic sediments leading to river nitrite accumulation. Appl. Environ. Microbiol. **63:**4679–4685.
32. **Kielemoes, J., P. De Boever, and W. Verstraete.** 2000. Influence of denitrification on the corrosion of iron and stainless steel powder. Environ. Sci. Technol. **34:**663–671.
33. **Larsen, J.** 2002. Downhole nitrate applications to control sulfate-reducing bacteria activity and reservoir souring, paper no. 02025. Proceedings of Corrosion/2002. NACE International, Houston, TX.
34. **Larsen, J., S. Zwolle, B. V. Kjellerup, B. Frolund, J. L. Nielsen, and P. H. Nielsen.** 2005. Identification of bacteria causing souring and biocorrosion in the Halfdan Field by application of new molecular techniques, paper no. 05629. Proceedings of Corrosion/2005. NACE International, Houston, TX.
35. **Larsen, L. H., T. Kjær, and N. P. Revsbech.** 1997. A microscale NO_3^- biosensor for environmental applications. Anal. Chem. **69:**3527–3531.
36. **Lee, W., and D. de Beer.** 1995. Oxygen and pH microprofiles above corroding mild steel covered with a biofilm. Biofouling **8:**273–280.
37. **Li, Y.-H., and S. Gregory.** 1974. Diffusion of ions in sea water and in deep-sea sediments. Geochim. Cosmochim. Acta **38:**703–714.
38. **Little, B., J. Lee, and R. Ray.** 2007. A review of "green" strategies to prevent or mitigate microbiologically influenced corrosion. Biofouling **23:**87–97.
39. **Ludwig, W., O. Strunk, R. Westram, L. Richter, H. Meier, Yadhukumar, A. Buchner, T. Lai, S. Steppi, G. Jobb, W. Forster, I. Brettske, S. Gerber, A. W. Ginhart, O. Gross, S. Grumann, S. Hermann, R. Jost, A. Konig, T. Liss, R. Lussmann, M. May, B. Nonhoff, B. Reichel, R. Strehlow, A. Stamatakis, N. Stuckmann, A. Vilbig, M. Lenke, T. Ludwig, A. Bode, and K.-H. Schleifer.** 2004. ARB: a software environment for sequence data. Nucleic Acids Res. **32:**1363–1371.
40. **Lueders, T., M. Manefield, and M. W. Friedrich.** 2004. Enhanced sensitivity of DNA- and rRNA-based stable isotope probing by fractionation and quantitative analysis of isopycnic centrifugation gradients. Environ. Microbiol. **6:**73–78.
41. **Mueller, R. F., D. Goeres, P. Sturman, and J. Sears.** 1998. Using microbial dynamics of *in situ* consortia in hydrocarbon reservoirs for the inhibition of souring. In K. L. Sublette (ed.), Proceedings of the 5th International Petroleum Environmental Conference. Integrated Petroleum Environmental Consortium and the University of Tulsa, Tulsa, OK.
42. **Muyzer, G., A. Teske, C. O. Wirsen, and H. W. Jannasch.** 1995. Phylogenetic relationships of *Thiomicrospira* species and their identification in deep-sea hydrothermal vent samples by denaturing gradient gel electrophoresis of 16S rDNA fragments. Arch. Microbiol. **164:**165–172.
43. **Myhr, S., B. L. P. Lillebo, E. Sunde, J. Beeder, and T. Torsvik.** 2002. Inhibition of microbial H_2S production in an oil reservoir model column by nitrate injection. Appl. Microbiol. Biotechnol. **58:**400–408.
44. **Nemati, M., T. J. Mazutinec, G. E. Jenneman, and G. Voordouw.** 2001. Control of biogenic H_2S production with nitrite and molybdate. J. Ind. Microbiol. Biotechnol. **26:**350–355.
45. **Nielsen, L. P.** 1992. Denitrification in sediment determined from nitrogen isotope paring. FEMS Microbiol. Ecol. **86:**357–362.
46. **Nielsen, M., L. H. Larsen, M. S. M. Jetten, and N. P. Revsbech.** 2004. Bacterium-based NO_2^- biosensor for environmental applications. Appl. Environ. Microbiol. **70:**6551–6558.
47. **Nogi, Y., S. Hosoya, C. Kato, and K. Horikoshi.** 2004. *Colwellia piezophila* sp. nov., a novel piezophilic species from deep-sea sediments of the Japan Trench. Int. J. Sys. Evol. Microbiol. **54:**1627–1631.
48. **Nuester, J.** 2005. New methods in biogeochemistry: the development of electrochemical tools for the measurement of dissolved and solid state compounds in natural systems. Ph.D. thesis. University of Bremen, Bremen, Germany.
49. **Peltzer, E. T., and P. G. Brewer.** 1993. Some practical aspects of measuring DOC: sampling artifacts and analytical problems with marine samples. Mar. Chem. **41:**243–252.
50. **Reinsel, M. A., J. T. Sears, P. S. Stewart, and M. J. McInerney.** 1996. Control of microbial souring by nitrate, nitrite or glutaraldehyde injection in a sandstone column. J. Ind. Microbiol. **17:**128–136.
51. **Rempel, C. L., R. W. Evitts, and M. Nemati.** 2006. Dynamics of corrosion rates associated with nitrite or nitrate mediated control of souring under biological conditions simulating an oil reservoir. J. Ind. Microbiol. Biotechnol. **33:**878–886.
52. **Revsbech, N. P.** 1989. An oxygen microelectrode with a guard cathode. Limnol. Oceanogr. **34:**472–476.
53. **Revsbech, N. P., and B. B. Jørgensen.** 1986. Microelectrodes: their use in microbial ecology. Adv. Microb. Ecol. **9:**293–352.
54. **Revsbech, N. P., and J. Sørensen.** 1990. Combined use of the acetylene inhibition technique and microsensors for quantification of denitrification in sediments and biofilms, p. 259–275. *In* N. P. Revsbech and J. Sørensen (ed.), Denitrification in soil and sediment. Plenum Press, New York, NY.
55. **Rickard, D., I. B. Butler, and A. Oldroyd.** 2001. A novel iron sulphide mineral switch and its implications for Earth and planetary science. Earth Planet. Sci. Lett. **189:**85–91.
56. **Rickard, D., and G. W. Luther.** 2007. Chemistry of iron sulfides. Chem. Rev. **107:**514–562.
57. **Rittmann, B. E.** 2004. Biofilms in the water industry, p. 359–378. *In* M. Ghannoum and G. A. O'Toole (ed.), Microbial biofilms. ASM Press, Washington, DC.
58. **Roe, F. L., Z. Lewandowski, and T. Funk.** 1996. Simulating microbiologically influenced corrosion by depositing extracellular biopolymers on mild steel surfaces. Corrosion **52:**744–752.
59. **Ryan, M. P., D. E. Williams, R. J. Chater, B. M. Hutton, and D. S. McPhail.** 2002. Why stainless steel corrodes. Nature **415:**770–774.
60. **Sandbeck, K. A., and D. O. Hitzman.** 1995. Biocompetitive exclusion technology: a field system to control reservoir souring and increase production, p. 311–320. *In* R. Byrant and K. L. Sublette (ed.), 5th International Conference on Microbial Enhanced Oil Recovery and Related Biotechnology for Solving Environmental Problems. National Technical and Information Services, Springfield, VA.
61. **Sanders, P. F., and P. J. Sturman.** 2005. Biofouling in the oil industry. *In* O. Bernard and M. Magot (ed.), Petroleum microbiology. ASM Press, Washington, DC.
62. **Singleton, D. R., M. A. Furlong, S. L. Rathbun, and W. B. Whitman.** 2001. Quantitative comparisons of 16S rRNA gene sequence libraries from environmental samples. Appl. Environ. Microbiol. **67:**4374–4376.
63. **Stumm, W., and J. Morgan.** 1996. Measuring the redox potential in natural waters. *In* W. Stumm and J. J. Morgan (ed.), Aquatic chemistry: chemical equilibria and rates in natural waters, 3rd ed. Wiley-Interscience, New York, NY.
64. **Sunde, E., B. L. P. Lilebo, G. Bodtker, T. Torsvik, and T. Thorstenson.** 2004. H_2S inhibition by nitrate injection to the Gulfaks field, paper no. 04760. Proceedings of Corrosion/2004. NACE International, Houston, TX.
65. **Telang, A. J., S. Ebert, J. M. Foght, D. W. S. Westlake, G. E. Jenneman, D. Gevertz, and G. Voordouw.** 1997. Effect of nitrate injection on the microbial community in an oil field as monitored by reverse sample genome probing. Appl. Environ. Microbiol. **63:**1785–1793.
66. **Thorstenson, T., G. Bødtker, B. P. Lillebo, T. Torsvik, E. Sunde, and J. Beeder.** 2002. Biocide replacement by nitrate in seawater injection systems, paper no. 02033. Proceedings of Corrosion/2002. NACE International, Houston, TX.
67. **Tiedje, J. M.** 1988. Ecology of denitrification and dissimilatory nitrate reduction to ammonium, p. 179–244. *In* A. J. B. Zehnder (ed.), Biology of anaerobic microorganisms. Wiley, New York, NY.
68. **Till, B. A., L. J. Weathers, and P. J. J. Alvarez.** 1998. Fe(0)-supported autotrophic denitrification. Environ. Sci. Technol. **32:**634–639.
69. **Warembourgh, F. R.** 1993. N_2 fixation in soil and plant systems, p. 157–180.

In R. Knowles and T. H. Blackburn (ed.), Nitrogen isotope techniques. Academic Press, New York, NY.

70. **Yakimov, M. M., L. Giuliano, G. Gentile, E. Crisafi, T. N. Chernikova, W. R. Abraham, H. Lunsdorf, K. N. Timmis, and P. N. Golyshin.** 2003. *Oleispira antarctica* gen. nov., sp. nov., a novel hydrocarbonoclastic marine bacterium isolated from Antarctic coastal sea water. Int. J. Sys. Evol. Microbiol. **53:**779–785.
71. **Yumoto, I., K. Kawasaki, H. Iwata, H. Matsuyama, and H. Okuyama.** 1998. Assignment of *Vibrio* sp. strain ABE-1 to *Colwellia maris* sp. nov., a new psychrophilic bacterium. Int. J. Syst. Bacteriol. **48:**1357–1362.
72. **Zehnder, A. F. B., and W. Stumm.** 1988. Geochemistry and biogeochemistry of anaerobic habitats, p. 1–38. *In* A. J. B. Zehnder (ed.), Biology of anaerobic microorganisms. Wiley, New York, NY.